Infrared Physics & Technology 151 (2025) 106121

Contents lists available at ScienceDirect

Infrared Physics and Technology

journal homepage: www.elsevier.com/locate/infrared

Research paper

Laser-free and low-jitter Electro-Optic Sampling of FEL-based THz radiation by intrinsic ultrafast laserlike-pulses at FLASH☆

Seung-gi Gang [a], Ekaterina Jung [a], Nicholas H. Matlis [a], Nikola Stojanovic [b], Rui Pan [a,*]

[a] Deutsches Elektronen-Synchrotron DESY, Notkestr. 85, 22607 Hamburg, Germany
[b] DLR Institute of Space Research, Rutherfordstr. 2, 12489 Berlin, Germany

ARTICLE INFO

Keywords:
Free electron laser
Terahertz
EOS
Laser-free
Low-jitter
Diagnostics

ABSTRACT

The FLASH1 THz beamline at DESY produces intense multicycle THz undulator radiation, along with quasi-single cycle edge radiation. Characterizing the temporal profile of THz radiation generated by free-electron lasers (FELs) is challenging due to unavoidable timing jitter between the THz pulse and an external laser synchronized to the FEL master clock. Although Electro-Optic Sampling (EOS) is a powerful diagnostic technique for the FEL THz sources, this jitter limits the temporal resolution and spectral bandwidth, necessitating timing jitter correction. To address this, we introduce a laser-free and low-jitter diagnostic method, Afterburner EOS (ABEOS), which uses broadband laserlike-pulses generated with the THz radiation as a probe. ABEOS results demonstrate good consistency with calculations across two probe configurations: a sequence of 10 pulses and a single pulse. Furthermore, comparisons with conventional methods of scanning EOS with an external laser, single-shot EOS (SSEOS), and FTIR show strong and reliable agreement. This technique offers 'laser-free and low-jitter' THz waveform characterization as a simplified, accurate, and reliable alternative to conventional THz diagnostics, validated up to 2 THz with potential for application at higher frequencies.

1. Introduction

Many free-electron laser (FEL) facilities, much like synchrotron facilities, have established dedicated IR and THz beamlines to exploit FEL-specific features for advanced research utilizing THz sources in both narrow- and broadband spectra. Narrowband THz sources, typically from undulators, provide high spectral purity, tunability, and intensity, making them ideal for resonant excitation and selective probing of material modes. Examples of FEL facilities providing such narrowband, tunable THz radiation include FELIX [1], FELBE [2], FLASH [3,4], and NovoFEL [5], all of which support a broad range of user experiments in material science and spectroscopy using pump-probe experiments. Broadband THz sources offer a wide spectral range and strong electromagnetic peak fields with short pulse durations, making them suitable for pump-probe experiments on ultrafast dynamics, nonlinear effects, and high-field THz interactions. These capabilities are demonstrated at FERMI [6], FLASH [3,4], and TELBE [2]. Beyond these examples, facilities such as CLIO [7], PITZ [8] in Europe, LCLS-II [9] and Jefferson Lab FEL [10] in the United States, and SXFEL [11] in Asia have either designed for or are in the process of expanding their capabilities into the IR and THz regimes, thereby further enhancing the scope of FEL-based research.

The FLASH1 THz beamline at DESY [12,13] generates multicycle THz pulses with wavelength from 10 μm to 300 μm, pulse energy up to 150 μJ, bandwidth of 10%, and linear polarization from the THz undulator. Single-cycle edge radiation [14,15] with radial polarization generated from the dump magnet is also coupled into the THz beamline. The THz undulator, named 'Afterburner', reuses electron bunches after XUV generation, as shown in Fig. 1, providing intrinsic temporal synchronization between THz and XUV pulses with less than 5 fs timing jitter, which is advantageous for pump-probe experiments. In this geometry, THz and XUV are decoupled by a mirror with a central hole.

Advanced diagnostics at FLASH1 include THz pulse energy, arrival time, and spatial/temporal profiles, which are critical for accurately analyzing material dynamics under THz excitation. The temporal profile of THz radiation, an essential information for dynamics studies, can be characterized through Electro-Optic Sampling (EOS) [16]. This technique uses ultrafast optical pulses, typically from the external femtosecond laser, synchronized to the FEL with timing jitter on the order of 100 fs. The remaining timing jitter and drifts can be monitored by an additional instrument, so called Electro Optic Spectral Decoding (EOSD) [17], and subsequently corrected, improving the

☆ This article is part of a Special issue entitled: 'WIRMS 2024' published in Infrared Physics and Technology.

* Corresponding author.
E-mail address: rui.pan@desy.de (R. Pan).

https://doi.org/10.1016/j.infrared.2025.106121
Received 31 January 2025; Received in revised form 9 May 2025; Accepted 27 August 2025
Available online 3 September 2025

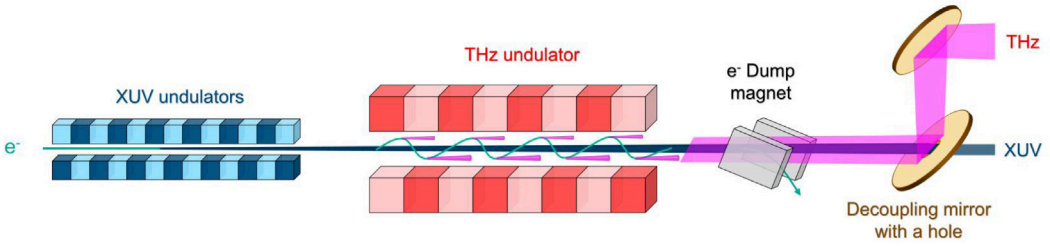

Fig. 1. Geometry of the undulators at FLASH1: A THz undulator, positioned downstream of the XUV undulators, generates intense, tunable, narrowband THz radiation from compressed electron bunches following XUV generation. Broadband edge radiation is also emitted at the electron dump magnet. Additionally, broadband spectra are produced as wiggler radiation from the THz undulator and as synchrotron radiation from the dump magnet.

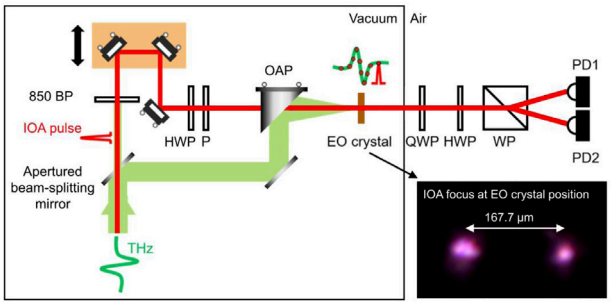

Fig. 2. The ABEOS configuration. The IOA, parasitically traveling with the THz radiation, is primarily used for EOS diagnostics. A small fraction of the IOA is reflected by an apertured beam-splitting mirror and used to assess the THz focus quality on the electro-optic (EO) crystal. The main power of the IOA passes through the beam-splitting mirror as a probe beam. The inserted picture shows two focal spots of the IOA, separated by 167.7 μm and measured by a CCD camera at the EO crystal position. The optics inside the black frame are mounted on an optical breadboard and can be pumped to vacuum. BP for bandpass filter, OAP for off-axis parabolic mirror, HWP for half-wave plate, QWP for quarter-wave plate, P for polarizer, WP for Wollaston prism, and PD for photo-diode.

overall synchronization to sub-10 fs [13]. Consequently, the temporal profile characterization of accelerator-based THz sources is complex and costly, which limits its widespread application.

To address these challenges, we propose Afterburner EOS (ABEOS), a novel laser-free and low-jitter diagnostic method. It utilizes Incoherent Optical Afterburner (IOA) radiation in near-infrared (NIR) spectral range from the FEL's THz undulator and dump magnet as a probe beam, intrinsically synchronized with the THz radiation. This eliminates the need for an external femtosecond laser source, synchronization, and jitter correction, offering a simplified and accurate THz diagnostic solution confirmed by comparison with other THz diagnostic methods. The ABEOS method has the potential to be a general diagnostic solution for FEL-based THz sources.

2. Experimental method

The FLASH1 THz undulator primarily generates coherent and intense THz radiation. With a high K-value of up to 49, it also operates in the wiggler regime, producing broadband incoherent synchrotron radiation, referred to as IOA, that extends to shorter wavelengths, including the VIS (visible) and NIR (near-infrared) spectral ranges. Furthermore, deflection of the electron bunch by the dump magnet's magnetic field generates synchrotron radiation up to visible spectrum. The IOA radiation from both the undulator and dump magnet, is transported through the same beamline as the THz beam. It is usually utilized for THz alignment and for assessing the THz focus quality on the EO crystal. The inset in Fig. 2 displays the IOA focal spots at the EO crystal position, following the THz beam path (green) in the ABEOS configuration. The focal spots were captured by a CCD camera without any filter. Each spot exhibits a Gaussian shape, which is resulting from radiation emitted during each half-period of the sinusoidal motion of electrons through the THz undulator as shown in Fig. 1. The measured FWHM focal spot size is in a range from 25.4 μm to 34.9 μm, with a separation of 167.7 μm at 150 μm of nominal THz wavelength. Since both the THz and IOA in the same optical beam path are focused using a reflective off-axis parabolic (OAP) mirror, they share the same focal length. The high-quality IOA focus therefore validates the THz focus. The IOA beam is usually filtered out by THz filters (e.g., 33 μm low-pass filter and various bandpass filters) in the THz branch. A typical THz focal size is measured to be between 200 to 300 μm depending on the nominal wavelength radiated from the THz undulator [13].

A new 'laser-free' approach to THz diagnostics uses the IOA as an alternative to an external laser, while the inherent synchronization between the IOA and THz pulses enables 'low-jitter' EOS diagnostics. The ABEOS setup is located at the end of the THz beamline and is shown in Fig. 2. The main part as shown in the black frame was built on a 450 mm × 300 mm breadboard with compact optics for improved mobility, and can be pumped into vacuum. The rest balanced detection part is always outside the chamber in air. At the entrance of the ABEOS setup, the IOA with lower divergence remains at the center within the THz radiation and is consequently separated from the THz pulse by passing through an aperture, 7 mm in diameter, of a beam-splitting mirror. After focusing both the THz and IOA pulses onto an EO crystal respectively, polarization changes in the IOA induced by THz electric field are monitored by a balanced detection scheme. The two separated beams with orthogonal polarizations after a Wollaston prism are focused by lenses with a 50 mm focal length and detected by two silicon-biased detectors (Thorlabs DET10A/M) with a 1 mm-diameter circular active area. The signal from each detector is amplified by a Phillips Scientific 6954 amplifier and collected by NI VirtualBench. The signals are later assigned as I_a and I_b, respectively, in Section 4.2. In the data post-processing, the difference signal from the two detectors is obtained and normalized by the total intensity of each IOA pulse. In the path of the IOA probe, an 850 nm bandpass filter with a 40 nm bandwidth is used to enhance the signal-to-noise ratio (SNR) of measured signal by eliminating other spectral components that could contribute to noise. The selected NIR also fulfills the phase-matching condition for EOS in the ZnTe crystal. Two lenses were used for collimating the IOA probe to half of its original beam size, followed by a third lens with a 150 mm focal length to focus it on the EO crystal. As a consequence, the focal size of the IOA for sampling is around 100 μm, while the THz focal spot is between 200 to 300 μm. Only one of the two IOA spots at the focus overlaps with the focused THz beam. The other IOA spot, which is not modulated by the THz beam in the EO crystal, is eliminated as background via the balance detection scheme.

Fig. 3 shows spectral components of the IOA obtained with and without the 850 nm bandpass filter. The bandpass filter transmits over 90% of the NIR spectrum near 850 nm, but allows some spectral leakage between 1320 and 1650 nm. The photon energy at 1550 nm (~0.80 eV) is too low to excite the electrons across the bandgap in

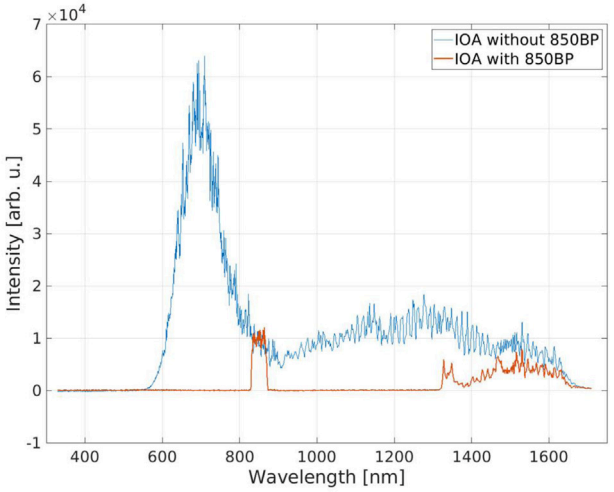

Fig. 3. Spectra of IOA radiation with (red) and without (blue) an 850 nm bandpass filter when the THz undulator is set at a nominal wavelength of 148.9 μm.

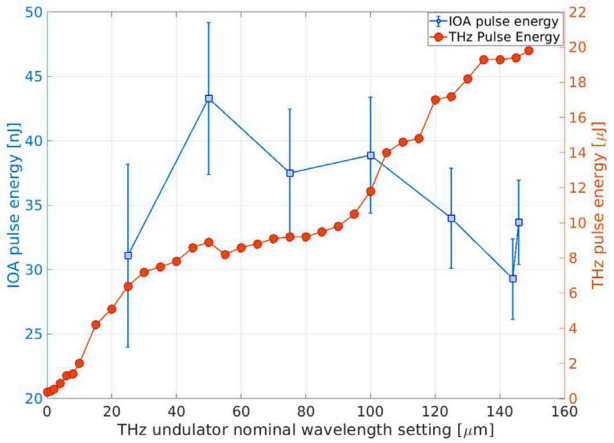

Fig. 4. THz and IOA pulse energy with varying THz undulator tunes. The IOA pulse energy was measured without the 850 nm bandpass filter.

silicon (~1.12 eV). As the Si-biased detectors were used in the ABEOS diagnostics, it has been also experimentally confirmed to show no response at 1550 nm. The spectral leakage has no contribution in the ABEOS signal.

The pulse energy of the THz radiation and its corresponding IOA are shown in Fig. 4. The IOA exhibited pulse energy in the tens of nJ range across varying THz undulator tunes. Its pulse energy decreased to several nJ after adding the 850 nm bandpass filter. Despite this reduction, the filtered pulse energy remained sufficient for EOS. However, due to the low pulse energy and incoherence of the IOA, its temporal structure could not be directly measured using techniques such as FROG or autocorrelation under the conditions of 45 pulses per burst, a repetition rate of 200 kHz, and a burst repetition rate of 10 Hz. Instead, the pulse duration was inferred to be in a similar range as the electron bunch length, measured between 90 and 130 fs at 560 MeV electron beam energy [18].

3. ABEOS calculation

Prior to the experiment, ABEOS results were estimated by calculations to demonstrate the proof of principle. To model THz pulses from the THz undulator at FLASH, 10 periods of THz cycles were set in the temporal profile with a nominal wavelength of 150 μm, as shown in Fig. 5(b). The THz pulse shape is in a square-like shape due to high K value of the THz undulator [19]. The THz transmission spectrum through air over a 2-meter propagation path, obtained from [20], is shown in Fig. 5 (d.3) and is applied to reproduce the THz profile in air. The IOA from the THz undulator comprises 10 pulses, separated by 500 fs, corresponding to a 150 μm undulator wavelength, as shown in Fig. 5(a). Each IOA pulse, after filtering, was centered at 850 nm. Each pulse duration is initially 100 fs in FWHM, but chirped to 106 fs by two pieces of 0.5-mm-thick diamond windows in the THz transport line. Among the 10 pulses, the electric field phase is random from one pulse to another. Two primary scenarios were examined: one with a single probe pulse from the dump magnet and the other one with a sequence of 10 pulses from the undulator, as described above. When it comes to a 1-pulse probe, as using an external laser, the ABEOS result should be the same as that obtained from the conventional EOS. The result accurately reflects the temporal profile of the THz field. In the case of 10-pulse probe from the undulator, the calculation can provide insight into the expected temporal profile by ABEOS and the corresponding spectrum. This analysis can be compared with the measured ABEOS profile and spectrum. A ZnTe crystal with 200 μm thickness was assumed in the calculation. The calculation included phase matching of the two optical beams in the crystal and the geometry of the electro-optic setup, following the methods in [21]. The results are shown in Fig. 5.

In Fig. 5, (a) shows the defined real part of the electric field for the 1-pulse probe and 10-pulse probe, with chirp induced by the diamond windows in the THz beamline. (b) shows defined THz profile in vacuum (top) and calculated THz profile after propagating through 2 m of air (bottom). The THz profile in air shows elongation in time, exceeding 20 ps, due to air absorption. The phase of air transmission spectrum was estimated from its spectral intensity in (d.3), based on the Kramers–Kronig relationship. The full information of the transmission spectrum is used to calculate the THz temporal profile in air. Using the 10-pulse probe in (a) and THz pulses in (b), the ABEOS profiles in vacuum and air in (c) are calculated. The probe with 10-pulse-IOA produces ABEOS profiles with significantly altered shapes (c.1 and c.2) compared to the original THz profiles in (b). These alterations are the result of the summed contributions of each pulse, with a certain delay between the pulses. Consequently, the ABEOS profiles measured with the 10-pulse probe do not directly reflect the original THz temporal profile. As shown in (d), in the frequency domain, the Fourier-transformed THz spectra obtained from the ABEOS signals with altered temporal profiles by 10-pulse probe (d.1-blue and d.2-orange) exhibit the main peak at 2 THz corresponding to the central frequency of the original THz spectrum (d.1-magenta and d.2-lime) derived from (b). The ABEOS spectrum represents the original THz spectrum. This occurs because the probe pulse delay contributes only in the phase of the spectrum but vanishes in the intensity. The spectrum in air, particularly, the main peak shows multiple spikes which correctly represent the air transmission in (d.3). Note that calculations with a single IOA pulse, producing an ABEOS temporal profile and spectrum identical to those of the original THz pulse, are not included in Fig. 5. These calculation parameters for the IOA and THz were selected to predict the anticipated ABEOS response and enable comparison with experimental results.

4. Results

4.1. THz characterization by ABEOS

THz temporal profiles were measured by the ABEOS methods both in air and in vacuum in separate beamtimes. During the measurements, the nominal wavelengths of the THz undulator were set near 150 μm. A 200 μm-thick ZnTe crystal was used. The results are compared with the conventional EOS result obtained in vacuum, shown in Fig. 6(a). For the

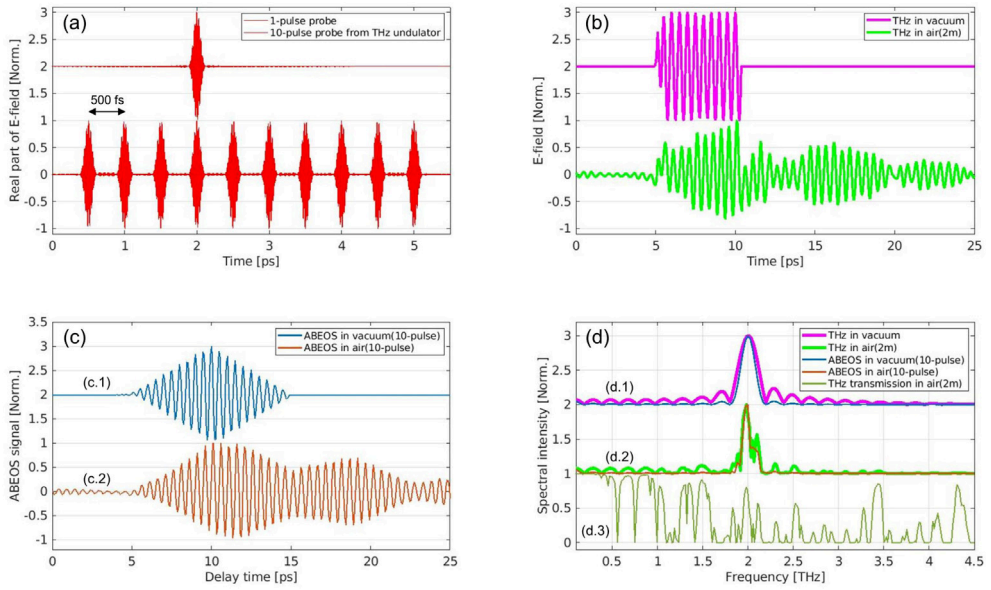

Fig. 5. ABEOS calculations. (a) Defined temporal profiles of the probes: a 1-pulse probe (top) and 10-pulse probe from the THz undulator (bottom) with 500 fs spacing, corresponding to the period of THz radiation at 150 μm. A chirp for the probe beam introduced by two 0.5-mm-thick diamond windows is included in the calculation. (b) Defined temporal profile of the THz pulse at 150 μm in vacuum (top) and calculated temporal profile after propagating through 2 m of air (bottom). (c) Calculated ABEOS signals: with the 10-pulse probe in vacuum (c.1) and in air (c.2) (d) Fourier-transformed THz spectral comparison: ABEOS spectrum (blue and orange) with the 10-pulse probe and the original THz spectrum (magenta and lime) in vacuum (d.1) and air (d.2), respectively. (d.3) shows spectral transmission of THz after propagation through 2 m of air.

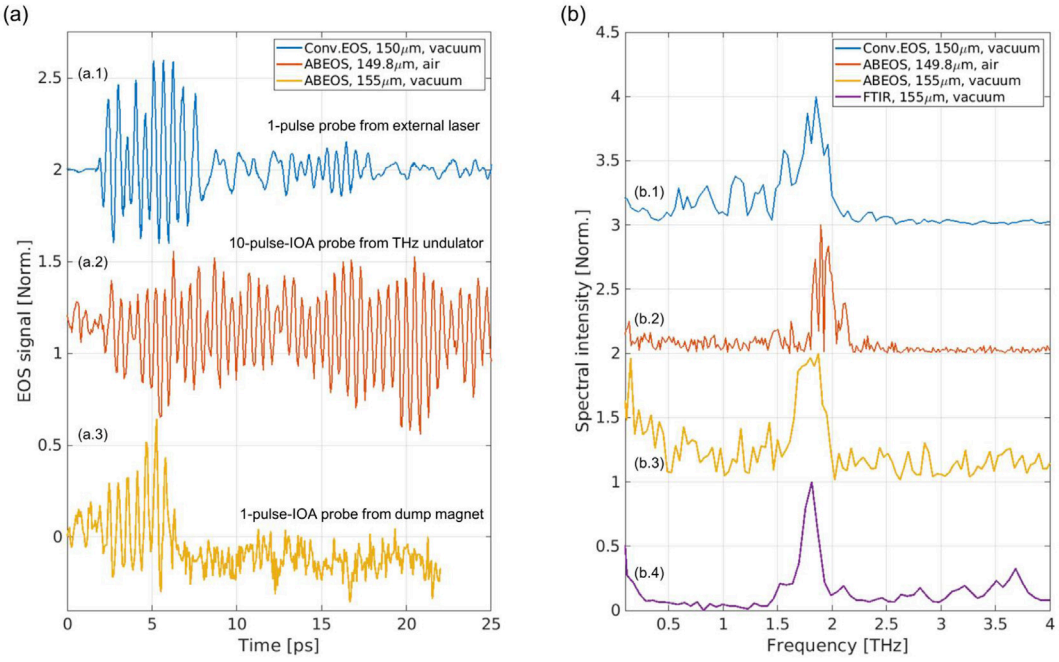

Fig. 6. Temporal profiles and spectra of THz undulator radiation with nominal wavelength settings near 150 μm. (a) Temporal profiles measured by conventional EOS with a 1-pulse probe from an external laser in vacuum as a reference (a.1), and ABEOS signals measured with 10-pulse-IOA probe from the THz undulator in air (a.2) and ABEOS signal measured with a 1-pulse-IOA probe from the dump magnet in vacuum (a.3). (b) Spectra obtained from conventional EOS (b.1), ABEOS in air (b.2), ABEOS in vacuum (b.3), and FTIR (b.4). The ABEOS and FTIR spectra (b.3 and b.4) were measured in vacuum for THz radiation in the same beamtime.

conventional EOS, an external laser with central wavelength of 830 nm and pulse duration of 21 fs was used as the probe. Their Fourier-transformed spectra from (a) are shown in Fig. 6 (b.1–3), along with the spectrum measured by FTIR (Fourier Transform Infrared Spectroscopy) (b.4) for comparison.

As shown in Fig. 6, the ABEOS profile in air (a.2) shows significant temporal elongation, compared with the conventional EOS (a.1). This elongation can be attributed to two factors: air absorption and the use of the 10-pulses probe in the ABEOS setup, as expected in the ABEOS calculation section. The spectrum of the ABEOS result successfully

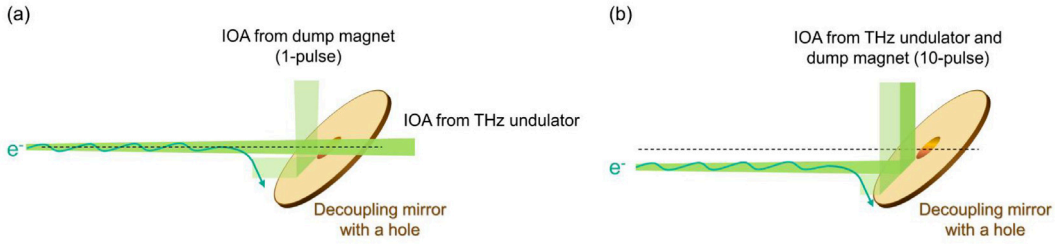

Fig. 7. Two electron beam configurations: (a) Electron bunch centered in the THz undulator, leading to mainly the single-pulse IOA from dump magnet coupled into THz transmission. (b) Electron bunch off-centered in the THz undulator, resulting in mainly the 10-pulses IOA from the undulator coupled into THz transmission.

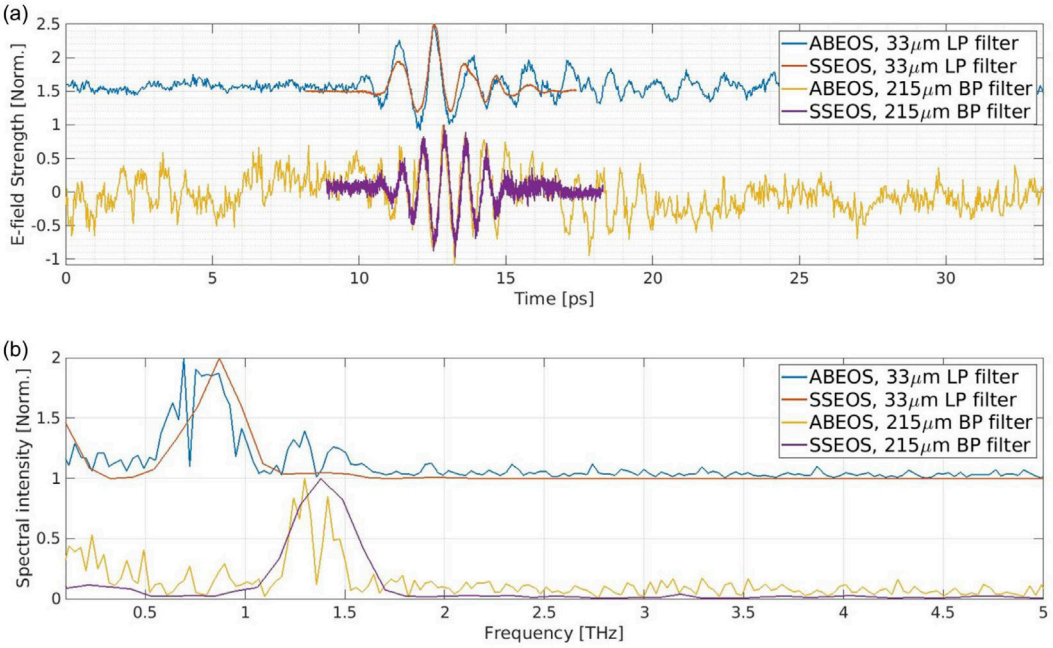

Fig. 8. Comparison of ABEOS and SSEOS: (a) Temporal profiles and (b) Spectra of the THz edge radiation measured by ABEOS and SSEOS using a 33 μm low-pass filter or a 215 μm band-pass filter.

reproduces the THz spectrum with a central frequency corresponding to the nominal THz wavelength.

In order to avoid air absorption, ABEOS measurement were performed in vacuum in another beamtime as shown in (a.3). The result has shorter temporal profile, closely resembling the original THz pulse. The asymmetry in the ABEOS profile (a.3) in vacuum results from imperfect signal balancing after pumping down the system. However, the measured profile is shorter than the expected calculation as in Fig. 5 (c.1). The results in Fig. 6 (a.2, a.3) imply that different types of IOA probes were selected for the measurements in the two beamtimes.

During the beamtime of ABEOS measurements in air shown in Fig. 6 (a.2), the electron beam was intentionally shifted off-center at the entrance and the exit of the THz undulator, while remaining parallel to its axis as shown in Fig. 7(b). Thus, most power of the 10-pulse-IOA probe from the undulator was coupled into the THz beamline, resulting in higher signal levels and improved SNR. As 10-pulse-IOA probe was employed for the ABEOS diagnostics, the signal was elongated over time shown in Fig. 6 (a.2), forming a similar envelope shape of calculated ABEOS profile under the same condition in Fig. 5 (c.2). While during the beamtime of ABEOS measurements in vacuum in Fig. 6 (a.3), the electron bunch was well-centered along the undulator axis, allowing the IOA from the THz undulator, with its lower divergence, to pass through the hole of the decoupling mirror as shown in Fig. 7(a). Only the 1-pulse-IOA probe, originating from synchrotron radiation from the dump magnet, was coupled into the THz beamline and used for the diagnostics. This setup reflects the configuration of the conventional EOS. Consequently, the measured ABEOS signal provides an accurate representation of the THz electric field profile like the conventional EOS.

In Fig. 6(b), the THz spectrum from ABEOS (b.3) is compared with the FTIR spectroscopy result (b.4) for the THz source under the same condition in vacuum. It shows good consistency between the two methods. In the ABEOS results with both the 1-pulse-IOA and the 10-pulse-IOA, the measured main peaks of the THz center frequency properly positioned at their assigned frequencies. The reliable performance of ABEOS has been demonstrated in measuring the THz spectrum. Even more notably, it has been shown to effectively measure the temporal profile when using the 1-pulse-IOA probe.

Additionally, with the THz undulator off, ABEOS measurements performed on the edge radiation from dump magnet using the 1-pulse-IOA probe (synchrotron radiation) is shown in Fig. 8. The results were compared with single-shot EOS (SSEOS) [22,23] measurements conducted in the same beamtime. Here, two different filters, 33 μm long-pass filter and 215 μm bandpass filter, were employed for the measurements. The 33 μm long-pass filter is transparent at spectral range below frequency of 9 THz. Since these measurements were performed in air, the ABEOS signal displays extended THz profile over tens of picoseconds due to air absorption. The parameters for SSEOS are defined by the laser pulse and the echelon reflector, which features temporal resolution of 50 fs and timing window of 10 ps. Therefore, the SSEOS

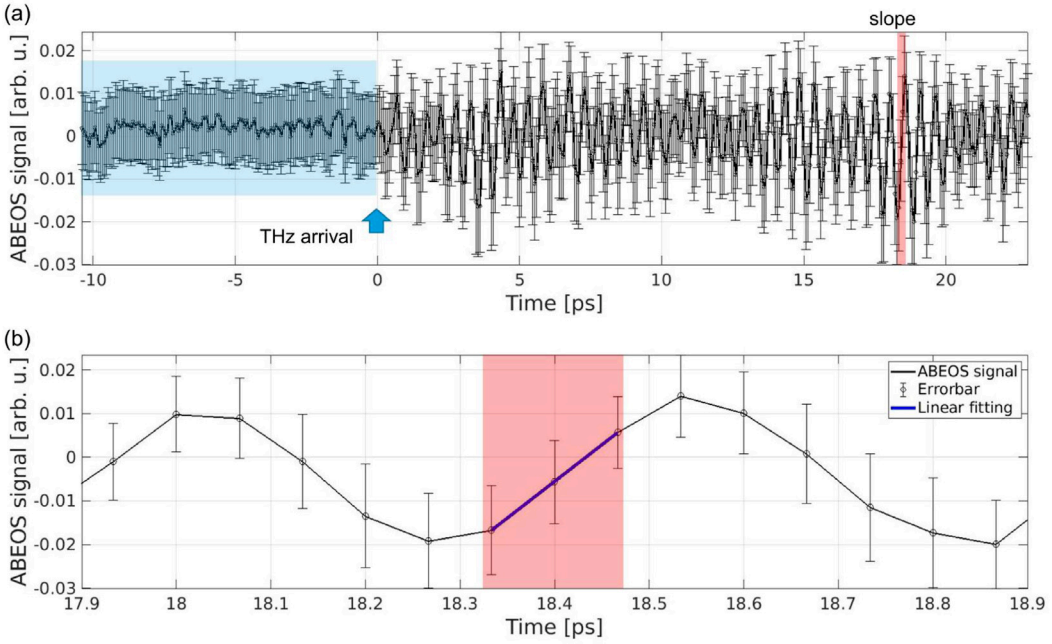

Fig. 9. Timing jitter measurement: (a) ABEOS signal of the THz pulse at 149 μm measured with a 200 μm thick ZnTe crystal. (b) Intensity fluctuations within the slope were used for timing jitter calculation. The timing jitter between the THz- and IOA pulses was estimated from the intensity fluctuations before (background in blue) and after the THz arrival (slope in red).

measurements cover only a portion of the ABEOS window around 10 ps, but profiles obtained from both diagnostics align well across different filters, achieving good temporal and spectral consistency. Thanks to the longer scanning window in time, the ABEOS measurements achieve better frequency resolution. Therefore, the air absorption is able to be seen in the ABEOS spectra. The spectra of both methods with 215 μm bandpass filter show consistent peak position corresponding to 1.4 THz as shown in Fig. 8.

4.2. Timing jitter in ABEOS

To evaluate the performance of this method, the timing jitter is estimated from the ABEOS signal in Fig. 9. During the scanning process, the ABEOS signal for each delay position is defined as $M_s = (I_a - I_b)/(I_a + I_b)$, where I_a and I_b are the intensities measured by detectors for two perpendicular polarizations in the balanced detection scheme. M_s is proportional to $E_{THz}(\tau)$, where E_{THz} is the THz electric field at the time-delay (τ) between the IOA probe pulse and the THz pulse. The jitter was determined by calculating the standard deviation of signal intensity, marked as ΔM, at given time-delay point. For this analysis, intensity fluctuations (ΔM) were extracted from the slope of the main peak, indicated in the red zone in Fig. 9, specifically considering the range from 10% to 90% of its magnitude. To estimate the timing jitter, we analyzed the local gradient of the rising edge after subtracting the baseline and the intensity fluctuation preceding the THz arrival. This gradient, determined by linear fitting and depicted in blue in Fig. 9(b), is denoted as k. The timing jitter was taken from the equation below

$$t_{jitter} = \frac{1}{k} * \sqrt{\Delta M_{slope}^2 - \Delta M_{bg}^2} \quad (1)$$

where $\Delta M_{\mathrm{slope}}$ represents the M_s fluctuations within the rising edge after THz arrival, and ΔM_{bg} refers to those in the background before THz arrival. With a 200 μm thick ZnTe crystal, we achieved a remarkably low timing jitter of 21.1 fs where the slope of the linear fit $k = 1.68 \times 10^{11}$ s^{-1}, $\Delta M_{slope} = 0.0093$ and $\Delta M_{bg} = 0.0086$. The observed jitter is attributed to practical limitations of the experimental method, such as imperfect signal balancing and fluctuations in the FEL THz pulse energy.

5. Conclusion

We have successfully demonstrated a novel "laser-free and low-jitter" THz electro-optic sampling (EOS) diagnostic technique, ABEOS, that utilizes the broadband IOA radiation generated with the THz pulse, bypassing the need for an external laser pulse. This approach is inherently free from laser-induced timing jitter. However, a residual timing jitter of 21 fs was observed, likely, due to practical experimental limitations contributed from intensity fluctuations. ABEOS calculations effectively corroborate the experimental results. ABEOS with the 1-pulse-IOA probe from the dump magnet shows accurately reproduced THz temporal profile. Although the ABEOS with the 10-pulse-IOA probe cannot directly represent the original THz temporal profile, as expected from the calculation, the spectra obtained using the ABEOS show precise THz information. The results have excellent agreement with other established diagnostic methods, including conventional EOS with an external laser, SSEOS, and FTIR spectroscopy. These results validate the capability of ABEOS for precise THz diagnostics in the frequency range up to 2 THz.

The developments of ABEOS will continue after the FLASH2020+ upgrade project [24]. With an expected enhancement in IOA intensity, further investigations become feasible, including direct measurement of the temporal profile of IOA pulses, testing the ABEOS on THz radiation with higher frequencies, implementing single-shot techniques in ABEOS for real-time monitoring, and studying IOA temporal and spatial coherence. This study underscores the potential of ABEOS as a robust and innovative diagnostic tool without complex optical setup, further leading to a low cost. The diagnostic method could be a general solution for the FEL-based THz sources.

CRediT authorship contribution statement

Seung-gi Gang: Writing – review & editing, Writing – original draft, Methodology, Formal analysis, Data curation. **Ekaterina Jung:** Writing – review & editing, Software, Methodology. **Nicholas H. Matlis:** Writing – review & editing, Methodology. **Nikola Stojanovic:** Writing – review & editing, Formal analysis, Conceptualization. **Rui Pan:** Writing – review & editing, Validation, Supervision, Methodology, Formal analysis, Conceptualization.

Declaration of competing interest

The authors declare that they have no known competing financial interests or personal relationships that could have appeared to influence the work reported in this paper.

Acknowledgments

The authors acknowledge support from DESY (Hamburg, Germany), a member of the Helmholtz Association HGF. We extend our gratitude to the colleagues at FLASH and Accelerator (M) Division for their support in scheduling beamtimes and ensuring the successful operation of FLASH.

Data availability

Data will be made available on request.

References

[1] W.J. van der Zande, R.T. Jongma, L. van der Meer, B. Redlich, FELIX facility: Free electron laser light sources from 0.2 to 75 THz, 2013 IRMMW-THz, 2013, pp. 1–2, http://dx.doi.org/10.1109/IRMMW-THz.2013.6665600.

[2] M. Helm, S. Winnerl, A. Pashkin, J.M. Klopf, J.-C. Deinert, S. Kovalev, P. Evtushenko, U. Lehnert, R. Xiang, A. Arnold, et al., The elbe infrared and thz facility at Helmholtz-Zentrum Dresden-Rossendorf, EPJ Plus 138 (2) (2023) 158, http://dx.doi.org/10.1140/epjp/s13360-023-03720-z.

[3] Z. Chen, C.B. Curry, R. Zhang, F. Treffert, N. Stojanovic, S. Toleikis, R. Pan, M. Gauthier, E. Zapolnova, L.E. Seipp, et al., Ultrafast multi-cycle terahertz measurements of the electrical conductivity in strongly excited solids, Nat. Commun. 12 (1) (2021) 1638, http://dx.doi.org/10.1038/s41467-021-21756-6.

[4] M. Riepp, A. Philippi-Kobs, L. Müller, W. Roseker, R. Rysov, R. Frömter, K. Bagschik, M. Hennes, D. Gupta, S. Marotzke, et al., Terahertz-driven coherent magnetization dynamics in labyrinth-type domain networks, Phys. Rev. B 110 (9) (2024) 094405, http://dx.doi.org/10.1103/PhysRevB.110.094405.

[5] O.A. Shevchenko, V.S. Arbuzov, N.A. Vinokurov, P.D. Vobly, V.N. Volkov, Ya. V. Getmanov, Ya. I. Gorbachev, I.V. Davidyuk, O.I. Deychuly, E.N. Dementyev, et al., The novosibirsk free electron laser-unique source of terahertz and infrared coherent radiation, Phys. Proced. 84 (2016) 13–18, http://dx.doi.org/10.1016/j.phpro.2016.11.004.

[6] P. Di Pietro, N. Adhlakha, F. Piccirilli, L. Capasso, C. Svetina, S. Di Mitri, M. Veronese, F. Giorgianni, S. Lupi, A. Perucchi, Terafermi: A superradiant beamline for THz nonlinear studies at the FERMI free electron laser facility, Synchrotron Radiat. News 30 (4) (2017) 36–39, http://dx.doi.org/10.1080/08940886.2017.1338423.

[7] J.M. Ortega, J.M. Berset, R. Chaput, F. Glotin, G. Humbert, D. Jaroszynski, P. Joly, B. Kergosien, J. Lesrel, O. Marcouillé, et al., Activities of the CLIO infrared facility, Nucl. Instrum. Methods Phys. Res. Sect. A 375 (1–3) (1996) 618–625, http://dx.doi.org/10.1016/0168-9002(95)01431-4.

[8] M. Krasilnikov, Z. Aboulbanine, G. Adhikari, N. Aftab, A. Asoyan, P. Boonpornprasert, H. Davtyan, G. Georgiev, J. Good, A. Grebinyk, et al., THz SASE FEL at PITZ: lasing at a wavelength of 100μm, J. Phys. Conf. Ser. 2687 (3) (2024) 032016, http://dx.doi.org/10.1088/1742-6596/2687/3/032016.

[9] Z. Zhang, A.S. Fisher, M.C. Hoffmann, Z. Huang, B.T. Jacobson, P.S. Kirchmann, W.S. Lee, A. Lindenberg, E.A. Nanni, S. Sasaki, et al., A High-Power, High-Repetition Rate THz Source for LCLS-II Pump-Probe Experiments, SLAC National Accelerator Lab., Menlo Park, CA (United States, 2019, http://dx.doi.org/10.18429/JACoW-FEL2019-WEP104.

[10] G.P. Williams, FAR-IR/THz radiation from the jefferson laboratory, energy recovered linac, free electron laser, Rev. Sci. Instrum. 73 (3) (2002) 1461–1463, http://dx.doi.org/10.1063/1.1420758.

[11] Y. Kang, H. Sun, K.Q. Zhang, C. Feng, Recent progress of THz source at the SXFEL, J. Phys. Conf. Ser. 2687 (3) (2004) 032011, http://dx.doi.org/10.1088/1742-6596/2687/3/032011.

[12] M. Gensch, L. Bittner, A. Chesnov, H. Delsim-Hashemi, M. Drescher, B. Faatz, J. Feldhaus, U. Fruehling, G.A. Geloni, Ch. Gerth, et al., New infrared undulator beamline at FLASH, Infrared Phys. Technol. 51 (5) (2008) 423–425, http://dx.doi.org/10.1016/j.infrared.2007.12.032.

[13] R. Pan, E. Zapolnova, T. Golz, A.J. Krmpot, M.D. Rabasovic, J. Petrovic, V. Asgekar, B. Faatz, F. Tavella, A. Perucchi, S. Kovalev, B. Green, G. Geloni, T. Tanikawa, M. Yurkov, E. Schneidmiller, M. Gensch, N. Stojanovic, Photon diagnostics at the FLASH THz beamline, J. Synchrotron Radiat. 26 (3) (2019) 700–707, http://dx.doi.org/10.1107/S1600577519003412.

[14] G. Gianluca, K. Vitali, S. Evgeni, S. Evgeni, Y. Mikhail, Theory of edge radiation part I: Foundations and basic applications, Nucl. Instrum. Methods Phys. Res. Sect. A 605 (3) (2009) 409–429, http://dx.doi.org/10.1016/j.nima.2009.03.240.

[15] G. Gianluca, K. Vitali, S. Evgeni, S. Evgeni, Y. Mikhail, Theory of edge radiation. Part II: Advanced applications, Nucl. Instrum. Methods Phys. Res. Sect. A 607 (2) (2009) 470–487, http://dx.doi.org/10.1016/j.nima.2009.04.039.

[16] Q. Wu, X.-C. Zhang, Free-space electro-optic sampling of terahertz beams, Appl. Phys. Lett. 67 (24) (1995) 3523–3525, http://dx.doi.org/10.1063/1.114909.

[17] Z. Jiang, X.-C. Zhang, Electro-optic measurement of THz field pulses with a chirped optical beam, Appl. Phys. Lett. 72 (16) (1998) 1945–1947, http://dx.doi.org/10.1063/1.121231.

[18] H. Wiedemann, Synchrotron radiation physics, SLF: Accel. Phys. Instrum. Sci. (2020) 3–49, http://dx.doi.org/10.1007/978-3-030-23201-6.

[19] T. Golz, High Repetition Rate THz Characterization At 4 th Generation X-Ray Light Sources (No. DESY-THESIS–2019-001), Deutsches Elektronen-Synchrotron (DESY, 2019, https://inis.iaea.org/records/hjang-4wh13.

[20] Spectroscopy of Atmospheric Gases: https://spectra.iao.ru/.

[21] R. Pan, Electro-Optic Diagnostic Techniques for the CLIC Linear Collider (Ph.D. thesis), University of Dundee, 2015, https://discovery.dundee.ac.uk/en/studentTheses/electro-optic-diagnostic-techniques-for-the-clic-linear-collider.

[22] K.Y. Kim, B. Yellampalle, A.J. Taylor, G. Rodriguez, J.H. Glownia, Single-shot terahertz pulse characterization via two-dimensional electro-optic imaging with dual echelons, Opt. Lett. 32 (16) (2007) 1968–1970, http://dx.doi.org/10.1364/OL.32.001968.

[23] G.T. Noe, I. Katayama, F. Katsutani, J.J. Allred, J.A. Horowitz, D.M. Sullivan, Q. Zhang, F. Sekiguchi, G.L. Woods, M.C. Hoffmann, et al., Single-shot terahertz time-domain spectroscopy in pulsed high magnetic fields, Opt. Express 24 (26) (2016) 30328–30337, http://dx.doi.org/10.1364/OE.24.030328.

[24] M. Beye, S. Klumpp, B. Faatz, I. Hartl, C. Lechner, E. Ploenjes-Palm, E.A. Schneidmiller, S. Schreiber, K. Tiedtke, R. Treusch, M. Yurkov, W. Wurth, S. Duesterer, FLASH2020+ Upgrade of FLASH Conceptual Design Report, Deutsches Elektronen-Synchrotron Hamburg, 2020, http://dx.doi.org/10.3204/PUBDB-2020-00465.